Geomorphological landslide inventory map of the Daunia Apennines, southern Italy.

Francesca Ardizzone[1], Francesco Bucci[1], Mauro Cardinali[1]*, Federica Fiorucci[1], Luca Pisano[2], Michele Santangelo[1], Veronica Zumpano[2]

[1]CNR - IRPI, Via della Madonna Alta 126, 06128, Perugia, Italy
[2]CNR - IRPI, Via Amendola 122, 70126, Bari, Italy

*Correspondence to: Mauro Cardinali (mauro.cardinali@irpi.cnr.it)

Keywords

Landslide inventory map, geomorphology, landslides, Daunia, expert mapping, Southern Italy

Abstract

Detailed and accurate geomorphological historical landslide inventory maps are an invaluable source of information for many research topics and applications. Their systematic preparation worldwide has been advised by many researchers as it may foster our knowledge on landslides, their spatial and temporal distribution, their potential interaction with the built environment, their contribution to landscape dynamics, their response to climate change in the past. Due to the extreme variability of the morphological and radiometric elements that can reveal historical landslides, geomorphological historical landslide inventory maps are produced by expert interpretation, which makes it a time consuming and expensive process, which often discourages wide area mapping activities. In this paper we present a new geomorphological historical landslide inventory map for a 1,460 km^2 area in the Daunia Apennines, the northern-western sector of the Apulia (Puglia) region, in Southern Italy. The inventory contains 17,437 landslides classified according to relative age, type of movement and estimated depth. Landslides were mapped according to rigorous and reproducible criteria applied by two teams of expert photo-interpreters to two sets of stereoscopic aerial photographs taken in 1954/55 and 2003. The dataset consists of a digital archive publicly available at https://doi.pangaea.de/10.1594/PANGAEA.942427 (Cardinali et al., 2022).

1 Introduction

Landslides are widespread natural hazards that occur worldwide posing threat to population, structures and infrastructures, causing relevant economic damage to society (Donnini et al., 2017; Froude and Petley, 2018; Petley, 2012). Availability of information on landslides locations, types, and sizes is a key basic information for many activities, from research to emergency support and land planning. Nevertheless, expert landslide mapping is not an investment priority in many countries and institutions, hence homogeneous wide scale landslide maps are rare (Guzzetti et al., 2012; Bucci et al., 2021), although the

availability of a landslide inventory map is fundamental to the production of landslide hazard and risk maps (Thiery et al., 2020). As a result, several applications spanning from land management to susceptibility modelling that would benefit from more homogeneous and complete datasets rely on often poor or incomplete/inconsistent data.

Any landslide mapping activity assumes (i) that landslides leave discernible features on the territory, i.e., a "landslide signature" made by radiometric and morphologic elements (Fiorucci et al., 2018; Guzzetti et al., 2012; Santangelo et al., 2022), (ii) that, in case of use of remote sensing, the data used (e.g. images) portray them, (iii) that the technique adopted is adequate to the data used, and (iv) that the operator (or the automatic or semi-automatic classification system) is able to exploit those features to detect and map landslides. Therefore, any landslide mapping activity is affected by a degree of incompleteness and inconsistency that stems from these basic assumptions. Landslides can remain unnoticed since (i) features were cancelled by erosion, other landslides and/or human activity (Malamud et al., 2004), (ii) the type of image or its spectral and spatial resolution may be inadequate for some types or sizes of landslides or for some locations (e.g. slope orientation), (iii) interpreters or (semi-)automatic systems may be unable to map some landslides using certain images or techniques (e.g. lack of experience, poor or incorrect system training).

Landslide inventory maps (LIMs) are the simplest tools to represent landslides distribution in a territory. They usually display landslide locations preferably as polygons rather than points or lines which should be used only for scale representation issues. LIMs usually store landslide attributes such as type of movement, estimated time of occurrence, estimated depth, activity at the date of the observation if available, and other more detailed data depending on availability and on the scale of the work (Bucci et al., 2021; Guzzetti et al., 2012; Santangelo et al., 2015).

Different types of inventories can be prepared. Event inventories (E-LIMs, Antonini et al., 2002; Ardizzone et al., 2012; Donnini et al., 2017; Fiorucci et al., 2017; Harp and Jibson, 2017; Mondini et al., 2012; Santangelo et al., 2022) report landslides that were triggered by specific events (i.e., rainfall, rapid snowmelt, volcanic eruption, earthquake). Geomorphological inventories (G-LIMs) report landslides that can be recognised by geomorphologists usually from the expert interpretation of stereoscopic aerial photographs (Bucci et al., 2021; Cardinali et al., 2001; Guzzetti et al., 2012; Santangelo et al., 2015) but also LiDAR derived images are widely used (Niculiţă et al., 2016; Razak et al., 2013; Schulz, 2004; Van Den Eeckhaut et al., 2007). They can be seen as the result of many landslide events over thousands of years (Malamud et al., 2004). Multi-temporal landslide inventories (M-LIMs) include the information of G-LIMs and also report landslides that occurred in the last tens of years as visible on historical images available at (possibly) regular time steps of several years (Galli et al., 2008; Guzzetti et al., 2012; Zumpano et al., 2020).

G-LIMs can be prepared for wide areas and provide a fundamental source of information about landslides that occurred in the last tens of thousands years. This particular type of inventory is an invaluable source of data but is time consuming and requires a high level of training and experience to get accurate and reliable results (Guzzetti et al., 2012), which usually hampers the systematic preparation of G-LIMs at regional or even national/continent scale.

This paper presents a new G-LIM prepared for the Daunia mountains in Puglia Region, Southern Italy. For this area, historically affected by diffuse slow moving large landslides, the Regional government required the preparation of a new landslide inventory to overcome the inhomogeneity among the existing inventories in terms of spatial distribution of landslides and of techniques adopted and working and publication scales. The landslide inventory map was produced through the interpretation of two sets of stereoscopic aerial photographs, taken in 1954/55 and 2003, supplemented by targeted field checks. The new landslide inventory is an entirely original dataset openly accessible at https://doi.pangaea.de/10.1594/PANGAEA.942427 (Cardinali et al., 2022).

2 Study area

The study area extends for 1,460 km^2, in the northern-western sector of the Apulia (Puglia in Italian) region (Southern Italy) (**Figure 1**). The area corresponds to the Daunia Apennine, located in the external (i.e. eastern) part of the Southern Apennine fold and thrust belt system.

The southern Apennine is the result of compressive tectonic dynamics, characterised by an oblique collision of the Calabrian forearc with the Apulian margin (Filice and Seeber, 2019) evolved from an antecedent subductive phase of thrust-emplacement (Vitale et al., 2011; Vitale and Ciarcia, 2013). Currently, the external (eastern) margin preserves the compressive tectonics while the internal sector is characterised by an extensive dynamic with tension faults that dissect the pre-existent fold and thrust structure (Brozzetti et al., 2009; Schiattarella et al., 2003).

The western sector of the Daunia Apennine is characterised by a wide variety of formations, mainly clay-rich flysch lithologies having different mechanical properties, highly affected by folds and faults (Cotecchia et al., 2020; Losacco et al., 2021; Pellicani et al., 2014b), resulting in medium-to-high relief with the elevations ranging between 55 and 1152 m a.s.l., where the highest peak is represented by Monte Cornacchia. Morphologically, it is strongly influenced by both the prolonged tectonic stresses and by the differences in composition and erodibility, where selective erosion has alternatively produced gentler and rounded slopes on the more erodible clayey formations, and steep slopes cut on harder rocks. In this sector, the orography associated with the widespread presence of clay-rich materials and the intense deformation is the main cause of landslides (Ciarcia et al., 2003; Losacco et al., 2021; Spalluto et al., 2021; Wasowski et al., 2010; Zumpano et al., 2020). The eastern sector is characterised by the Sub-Apennine clay formation and alluvial deposits, and by gentle slopes slightly dipping towards NE. In this sector, several orders of terraced fluvial deposits overlay the sub-Apennine clay formation. Here, mass movements are mainly concentrated along the scarps of the terraces.

The Daunia Apennine is influenced by a Mediterranean sub-humid climate with mild and often wet winters and usually hot and dry summers. In general, inter-annual temperature variations are significant and the total yearly precipitation seldom

92 exceeds 1000 mm (Wasowski et al., 2012, 2010). In the area, torrential streams flow NE-SW, draining the sediments from the

93 Daunia Mountains, through the Tavoliere Plain towards the Adriatic Sea.

94 In response to the litho-structural and morpho-climatic setting of this area, landslides are widespread. They are mostly slow

95 moving slide-type and flow-type movements, involving soil and earth, and secondarily rock material. Rapid moving (i.e. debris

96 flows) and fast moving (i.e. rock falls) landslides are less abundant (Wasowski et al., 2010, 2012; di Lernia et al., 2022;

97 Zumpano et al., 2020) . The widespread presence of landslides in the area is a major cause of damage ~~Landslides are widespread~~

98 ~~in the area, especially in the western sector, where landslides are a major cause of damage~~ to urban settlements, to the road

99 network, and to the stability of buildings. These features determine a direct effect on the development and the economy of the

100 area (Pellicani et al., 2014b, a; Zumpano et al., 2020).
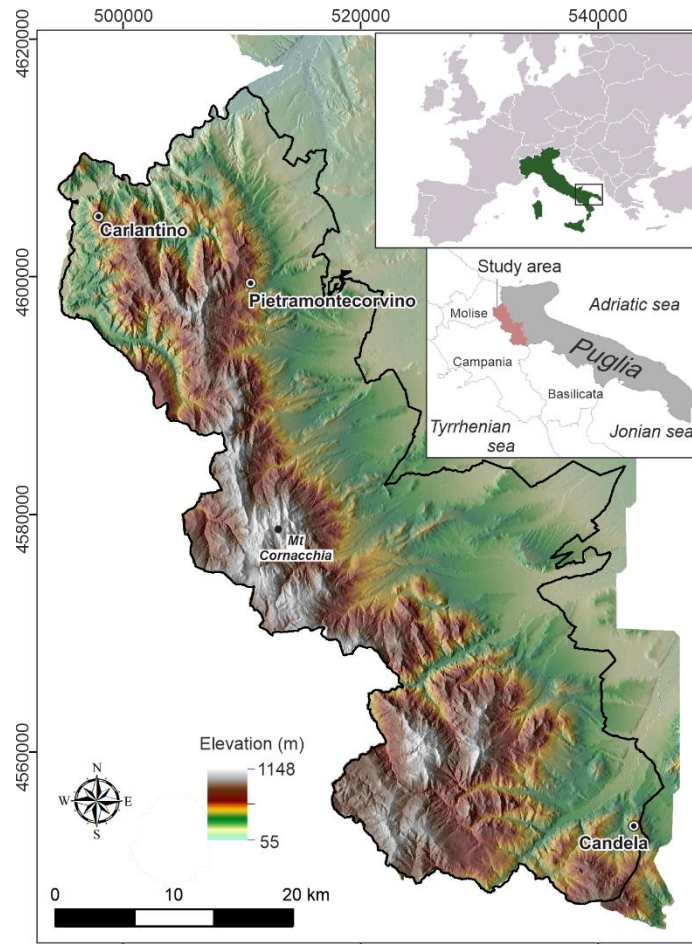
101

102 **Figure 1 -** Location map of the study area. Base map: DTM at 8 m resolution made available by the Regione Puglia
103 administration.

104

3 Materials and methods

The procedure adopted to prepare the landslide inventory map is illustrated in **Figure 2**. The overall procedure consists in three main phases: (i) data collection; (ii) photo-interpretation; and, (iii) editing. The entire work was carried out by a "mapping team" made up by four interpreters and one supervisor, and an "editing team" made by three GIS editors.

The first stage of the work consisted in the collection of data available for the study area (i.e., ancillary data, **Figure 2**; complete list in the Appendix A) and the pre-processing of the aerial-photographs to produce oriented stereo-models in absolute coordinates to be used for the visual interpretation in a photogrammetric GIS environment. Such photogrammetric pre-processing included the interior and exterior orientation of each pair of aerial photographs. For the interior orientation, a non-metric camera model was adopted for which the focal length of the camera, the flight altitude and the pixel size were required, while for the representation of the ground-to-image geometry (exterior orientation) Ground Control Points (GCPs) were used. The planimetric coordinates (x, y) of GCPs were manually chosen by visual comparison of the aerial photographs and an orthophoto available taken in 2006 (at 1 m resolution available for download at http://www.sit.puglia.it/) and 1988 (at 1 m resolution, available as WMS service at http://www.pcn.minambiente.it/mattm/servizio-wms/). The altimetric coordinate (z) of the GCPs were obtained from a Digital Elevation Model (8 m resolution available for download at http://www.sit.puglia.it/). Stereo models were prepared for both aerial photographs epochs, 1954/55 and 2003, i.e. the oldest and the latest aerial photographs acquisitions available for the entire study area.

The second phase of the work is the photo-interpretation (**Figure 2**) of the aerial photographs. At the very initial stage of the work, the entire mapping team defined a legend through an expeditious photo-interpretation in representative geomorphological settings and according to well-established landslide classifications schemas (Cruden and Varnes, 1996, Hungr et al., 2014, WP/WLI, 1993). Then, divided in pairs, for each stereo-pair the mapping team prepared a preliminary interpretation (1st level G-LIM in **Figure 2**) that was then reviewed by the supervisor and discussed with the mapping team. After this step, an updated version of the map was produced (2nd level G-LIM in **Figure 2**). Each of the two mapping team pairs performed their preliminary photo-interpretation in alternating strips along the flight plan. The side-lap between subsequent strips was therefore common between the different couples of interpreters, and it was used to compare, correct and homogenise the interpretation made by different sub-teams independently. Such a continuous interaction among geomorphologists made it possible to best define the characteristics of the identified landslides, limiting interpretation inconsistencies among operators. Finally, at significant advancement steps, extensive field checks were performed by the entire mapping team to check, validate and correct the inventory based on field evidence. After the field check stage, the interpretation phase was concluded and the landslide mapping considered quasi-definitive, i.e., occasional changes might be needed if inconsistencies were observed in the third stage (e.g., consistency with contour maps and hydrography).

The third and last step of the procedure, (editing) consists in the preparation of the geographical database. The interpreted features drawn as polylines by the mapping teams were verified on the digital topography, i.e., contour lines at scale 1: 5,000 (editing phase in **Figure 2**). The checked polylines were then converted into polygon features, and verified with topological

checks to avoid overlapping. Finally, the polygons were coded according to the adopted legend (legend description is available in Section 4 and the database schema is described in the metadata of the digital archive available at https://doi.pangaea.de/10.1594/PANGAEA.942427, Cardinali et al., 2022). Landslides recognised in the study area were classified by type according to Cruden and Varnes, (1996) and Hungr et al., (2014). Additionally, according to WP/WLI, (1993) landslides were classified based on the estimated depth (as shallow or deep-seated), and the inferred relative age (as relict, very old, old or recent). Examples and descriptions of landslides of different type, relative age, and depth, as well as of other geomorphological elements are detailed in Section 4. A more detailed explanation of the criteria used for the definition of the legend was given by Bucci et al., (2021).

3.1 Available data

The Geomorphological landslide inventory map (G-LIM) of Daunia Sub-Apennines was prepared through systematic visual interpretation of a set of 270 b/w stereoscopic aerial photographs taken in 1954/55 at 1: 33,000 scale and of 384 b/w stereoscopic aerial photographs taken in 2003 at 1: 30,000 scale. Aerial photographs were provided as 800 dpi scanned copies. All the ancillary data used for interpretation are listed and described in detail in Appendix A.

3.2 Hardware and software

For the interpretation phase we used the digital stereoscopic vision 3D PluraView System, composed of two monitors for the stereoscopic vision of digital images and a 45° inclined mirror placed on the bisector of the two monitors equipped with passive 3D glasses, (*https://www.3d-pluraview.com/en/*). A dedicated computer, equipped with IMAGINE Photogrammetry software (*https://www.hexagongeospatial.com/products/power-portfolio/imagine-photogrammetry*) was used for the pre-processing of digital stereoscopic images, and ArcGis software with the 3D Analyst extension tool, was used to digitise the 3D data in a GIS environment (Ardizzone et al., 2013; Fiorucci et al., 2015). The spatial resolution of the images (~1m for 1954/55 epoch, ~0.9m for 2003 images) and the zoom capability of the 3D PluraView System allow the identification of very small features. The stereo pairs were investigated using a zoom level at scale 1: 2500 to obtain mapped features compatible with a publication scale of 1: 5000. The capabilities of ERDAS IMAGINE ™ Photogrammetry Suite and ArcGIS ™ Stereo Analyst of preparing, managing and viewing multiple sets of oriented images all having the same reference system allowed the fast comparison of landscape features in different epochs, improving the interpretation.
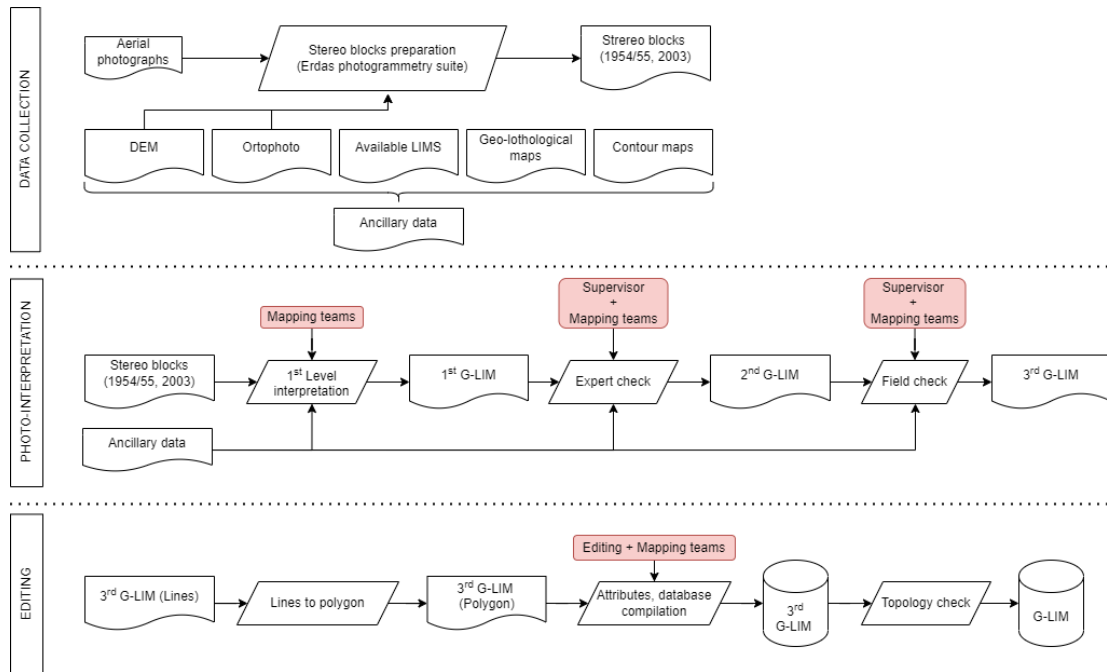
Figure 2. Flowchart of the procedure to prepare the geomorphological landslide inventory map. Pink rectangles indicate contributions of different teams/operators.

4 Geomorphological Landslide Inventory Map.

The inventory covers an area of 1,460 km^2 and include 17,347 landslides (**Figure 3**), corresponding to an average density of about 15.6 landslides per square kilometre (**Table 1**) if lowlands plains are excluded. Locally, landslide density reaches 60 landslides per square kilometre. Landslide size (Landslide Area, A_L in m^2) is in the range $1.9 \times 10^1 < A_L < 6.8 \times 10^6$ (**Table 1**). Overall, landslides cover an area of 442 km^2, which represents the 39% of the hilly and mountainous portion of the study area.

In this section the different groups of elements composing the inventory will be analytically described. Sections 4.1 to 4.3 describe landslides classified according to their relative age, type classification and estimated depth. Section 4.4 describes the widespread landslides (i.e. landslides represented as groups of failures due to their small size and high spatial frequency). Section 4.5 describes the descriptive statistics of the landslide inventory, and Section 4.6 presents the geomorphological elements (i.e. elements that are considered in relation with slope evolution and that can provide useful information for landslide identification and mapping).

Table 1. Descriptive statistics of landslides by relative age.

	Number of features	Total Area [m^2]	Minimum area [m^2]	Maximum area [m^2]
Very old relict landslides	37	8.85×10^7	1.38×10^5	6.78×10^6
Very old landslides	120	8.75×10^7	5.82×10^4	2.86×10^6
Pre-2003 landslides	14,793	3.39×10^8	7.1×10^1	2.3×10^6
Recent landslides (2003)	2,049	5.01×10^6	1.89×10^1	1.63×10^5
Widespread landslides	348	1.13×10^7	3.78×10^2	3.54×10^5
Entire inventory	17,347	$4.421.89 \times 10^8$	1.89×10^1	6.77×10^6

4.1 Landslide by relative age

Based on their appearance in aerial photographs, landslides were classified according to their relative age, namely: (i) very old relict landslides, (ii) very old landslides, (iii) old landslides, and (iv) recent landslides (**Figure 3**). The four relative age levels are the result of a major subdivision, referring to the general morphologic appearance of landslides (Keaton and DeGraff, 1996), and are based on the assumption that evidence of landslides become less obvious with the increasing age, due, for example, to erosion processes, vegetation growth, and occurrence of other landslides. Hence, older landslides are more difficult to detect than more recent ones.

Landslides modifications within the two epochs (1954 and 2003) were negligible for very old relict and very old landslides, whereas they were more frequent for old landslides (i.e. pre-2003). Therefore, the final landslide delineation considers by definition the latest evidence within the 49-year time interval.

In our G-LIM, the most represented landslides in the study area are old landslides (**Table 1, Figure 3C**), corresponding to 14,793 landslides covering a total landslide area of 339 km^2. Recent landslides (**Figure 3D**) are also very numerous (2,049) They are generally small, and cover a total area of 5 km^2. Very old relict and very old landslides (**Figure 3A, B**) are represented by 37 and 120 landslides respectively, and cover an area of 88 and 87 km^2. The feature of being fewer and larger than more recent landslides is common to other geomorphological inventories (Bucci et al., 2021, 2016a; Santangelo et al., 2015). The spatial relationships between landslides belonging to the relative age groups are displayed in **Figure 4**, where a representative example of the landslide relative age pattern for the entire inventory is shown.
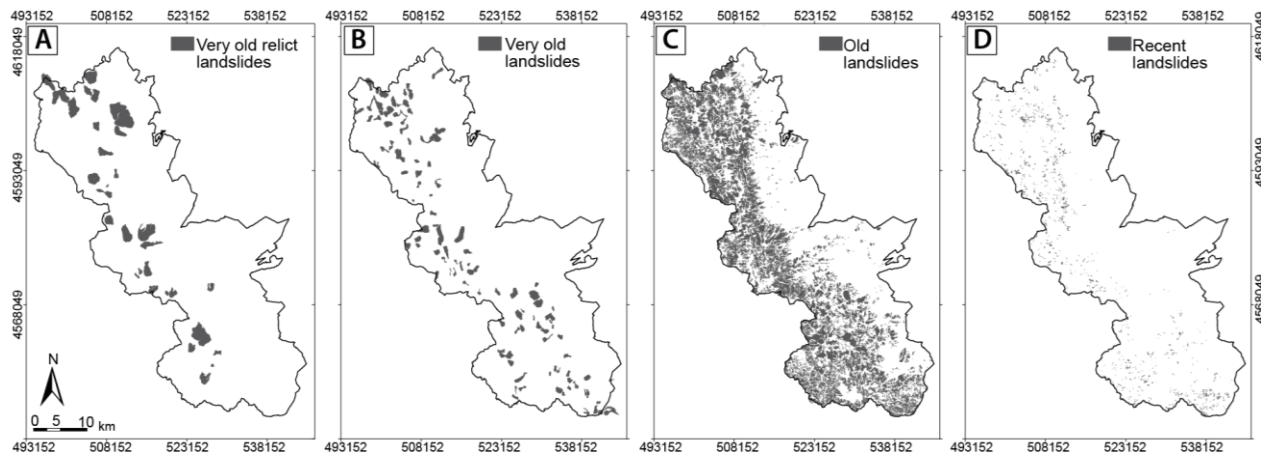
Figure 3. Spatial distribution of (A) very old relict landslides, (B) very old landslides, (C) old landslides and (D) recent landslides.

Figure 4B-E shows the inventory disaggregated according to the four relative age classes recognised. The sequence of the four panels represents a timeline, where landslides of each time step are shown with their own colour, the same as **Figure 4A**, whereas landslides belonging to antecedent time steps are represented in white.

In addition to the four mentioned relative age classes, a generation principle based on crosscut relationships, defines minor subdivisions within each age class: younger landslides cover the older ones. For the overall inventory, this criterion allowed us to detect up to: i) two landslides generations within the relict landslides, ii) two generations within the very old landslides, iii) four generations within the old landslides, iv) two generations within the recent landslides. Such minor subdivisions are applicable only to landslides that overlap, i.e. it is not applicable for landslides that do not overlap. For instance, in **Figure 4D** the age class "old" records up to three overlapping classes, indicated respectively in light orange (first failure "old"), orange (second failure "old") and red (third failure "old").
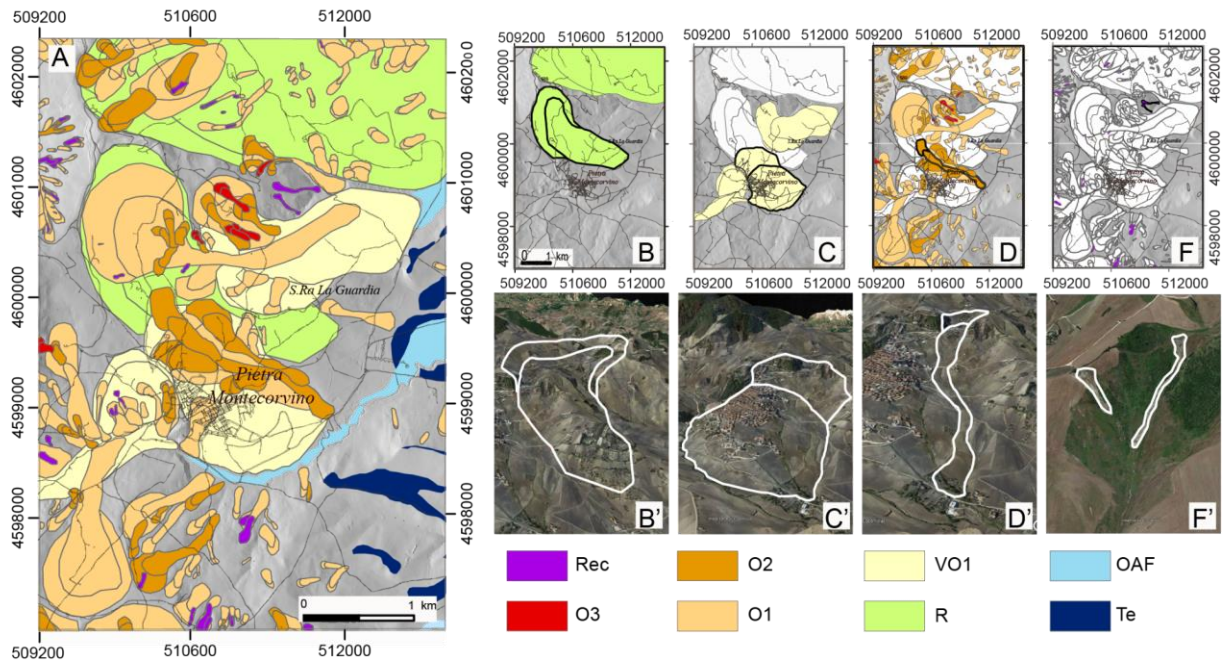
Figure 4 - Example of the relative age classes in the area of the Pietramontecorvino municipality (see **Figure 1** for reference). (A) Detail of the inventory in the selected location. Black outline polygon indicates the area in B to I. Very old relict landslides (B), very old landslides (C), old landslides (D), and recent landslides (E) are portrayed in detail. Black outlined polygons in B to E are represented singularly in a perspective view on © GoogleEarth™ in B' to F'. In the legend, Rec: Recent landslides; O1, O2, O3: old landslides of first, second and third generation; VO1: Very old landslides of first generation; R: relict landslides; OAF: old alluvial fan; Te: terrace.

214

215

216 Landslides classified as very old relict (**Figure 4B**) generally affect entire slopes, where the energy of the relief is greatest.
217 They are usually controlled by the geological and lithological structure and the presence of main faults (Bucci et al., 2016a).
218 Very old relict landslides are deeply dismantled by the erosive action of watercourses and often reshaped by recurring
219 gravitational phenomena. These morphological modifications are often related to the regional morphological and tectonic
220 evolution, which has determined considerable base level variations in the study area. As a consequence, these landslides are
221 often suspended with respect to the present day base level, and totally or partially isolated from the recent evolution of the
222 drainage network. Therefore, very old relict landslides are considered to have occurred under geomorphological and climatic
223 conditions different from the present day (WP/WLI, 1993).
224 Landslides classified as very old (**Figure 4C**) show evidence of active and passive interaction with river dynamics, being often
225 partly eroded from them and locally modifying their path. Also, morphological modifications of very old landslides can be
226 induced by the occurrence of other mass movements over time. Very old landslides are generally large and in agreement with
227 the present day river network, they are mainly distributed where the local relief is high and they often occur in or near very
228 old relict landslides, as local reactivations.

229 Landslides classified as old (**Figure 4D**) present recognizable evidence on both 1954/55 and 2003 aerial photographs epochs.

230 These landslides generally present morphological characteristics typical of landslides which are not modified by erosion (e.g.,

231 concave-convex shape of the slope, presence of steps and back slopes in the deposit area). Old landslides tend to cluster

232 spatially, as it is evident from the several generations of mass movements that were recognised. Spatial clustering of old

233 landslides is even more evident in the vicinity of very old or very old relict landslides. Old landslides are hypothesised to have

234 occurred in more recent time (yet undefined) compared to very old and very old relict landslides.

235 Landslides classified as recent (**Figure 4E**) are represented by landslides that show evidence of having occurred close to the

236 date of the 2003 aerial image. The diagnostic elements for the identification of recent landslides refer not only to the

237 morphological evidence but above all to the spectral elements (photographic tone and contrast) which can be perceived even

238 with a bi-dimensional (2D) view of the images. Recent landslides are mainly shallow failures essentially involving the soil

239 horizons or the alteration of the debris cover for a few metres in depth. Their spatial distribution is ubiquitous and only limited

240 to the areas where the triggering event induced the landslides. Therefore, they were found both in previously unaffected slopes

241 or within pre-existing landslides.

242 As opposed to the recent landslides, which evidence is stronger, some uncertainty characterises the delineation of older

243 landslide borders, which boundaries can be affected or even dismantled by different degrees of erosion, or covered by more

244 recent slope failures. General considerations on relative age criteria of classification (Keaton and DeGraff, 1996) support our

245 own experimental observations on landslide morphological appearance that the uncertainty degrees in landslide mapping

246 increase with the increasing landslide age (Bucci et al., 2021). However, we do not have information on absolute age of the

247 landslides in our study area, and only hypothesise that the majority of the mapped landslides occurred in the last 10–20 Kyr,

248 as suggested by findings of recent studies on landslide age in Southern Apennine (Gioia et al., 2011) and elsewhere (Niculiță

249 et al., 2016; Pánek et al., 2014).

250 **4.2 Landslide by type**

251 The type of the landslides is assigned based on the morphological and radiometric signature of each landslide on the aerial

252 photographs. Landslide types included in the legend of the G-LIM are (i) slide type landslides (which include deep seated rock

253 slides or earth slides, shallow soil slides or earth slides), (ii) earth flow, (iii) slide-earth flow, (iv) debris flow, (v) rock fall and

254 (vi) sackung (**Table 2**). In **Table 2**, widespread landslides refer to polygons representing groups of landslides whose size is

255 smaller than the smallest feature that can be represented at the publication scale of the final map.

256

257 **Table 2.** Descriptive statistics of landslides by type.

Landslide type	Number of features	Total Area [m^2]	Minimum area [m^2]	Maximum area [m^2]
Slide type	9,867	2.9×10^8	1.9×10^1	6.8×10^6
Earth flow	2,435	4.6×10^7	3.6×10^1	1.3×10^7

Slide-earth flow	4,657	1.6×10^8	8.8×10^1	2.9×10^6
Debris flow	38	6.5×10^5	1.4×10^2	1.4×10^5
Rock fall	1	6.0×10^4	6.0×10^4	6.0×10^4
Sackung	1	5.0×10^5	5.0×10^5	5.0×10^5
Total	16,999	4.3×10^8	1.9×10^1	1.3×10^7

Widespread landslide	**Number of features**	**Total Area [m^2]**	**Minimum area [m^2]**	**Maximum area [m^2]**
Shallow earth/soil slides and earth flows	138	7.1×10^6	5.2×10^2	3.5×10^5
Debris flow	193	4.1×10^6	3.8×10^2	1.4×10^5
Rock fall	17	1.3×10^5	5.2×10^2	2.4×10^4
Total	348	1.1×10^7	3.8×10^2	3.5×10^5

258

259 According to the type of movement, the most represented landslides in the study area are slides (9,867 landslides, **Figure 5A**)

260 covering a total landslide area of 287 km^2. The 4,657 slide-earth flows (**Figure 5B**) cover an area of 158 km^2, whereas earth

261 flows are represented by 2435 landslides (**Figure 5C**) covering an area of 46 km^2. **Table 2** reveals that these three classes

262 represent more than 95% of the total landslides, while debris flows (38), rock falls (1) and sackungs (1) are rare.

263

264 The main features of the three more represented landslide types are illustrated in **Figure 6**. Inspection of the figure highlights

265 the main cartographic differences (**Figure 6A, C, E**) between different landslide types (**Figure 6B, D, F**).

266 **Figures 6A, B** illustrates the slide type landslides. Such failures present a well-defined scarp which can be semi-circular

267 (rotational slides) or angular (translational slides). The slide deposit is convex, with a morphologically depressed head of the

268 deposit, characterised by a centripetal drainage and local counter-slopes, and a toe characterised by a typical upward bulge

269 (**Figure 6B**). It is reasonable to expect a volume balancing between escarpment and deposit areas since slides are usually

270 characterised by low mobility of landslide material. This is clear in **Figure 6A, B** that shows a planimetric and altimetric shift

271 of about 25 metres of the displaced material, with no evidence of chaotic rearrangement and/or volumetric changes.

272 Slide-earth flows (**Figure 6C, D**) initiate as slides, then evolving into flows. Therefore, they show the characteristics of slides

273 (most commonly rotational) in the escarpment area and in the head of the deposit, where local endorheic conditions can

274 promote seasonal swamps with diffuse organic soils development (**Figure 6C, D**). On the other hand, the transport zone and

275 accumulation zone are more similar to earth flows, characterised by the typical lobe shape of the accumulation zone (**Figure**

276 **6C, D**).
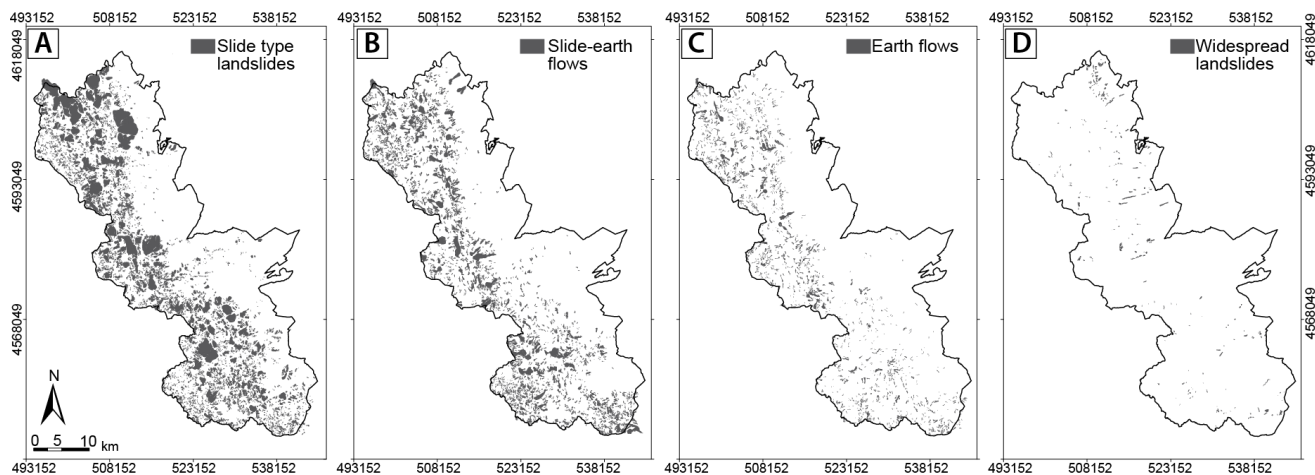
Figure 5. Spatial distribution of (A) slide type landslides, (B) slide-earth flows, (C) earth flows, (D) widespread landslides.

Earth flows (**Figure 6E, F**) are characterised by an overall elongated planar shape, with the median part narrower than detachment and accumulation zones. The mobility of earth flows is generally higher than slides, which is also evident in their more elongated shape. A typical earth flow is usually bounded by lateral streams draining the deposits into the main river valley, which typically experiences narrowing of the valley section and erosion on the opposite side of the landslide toe (**Figure 6F**)

Debris flows and rock falls are not statistically represented in our inventory because the Daunia Apennine lacks the environmental conditions favouring their development, such as steep rocky slopes and sub-vertical cliffs. However, local geomorphological conditions (e.g. steep edges of suspended fluvial terraces) can promote the formation of coalescing phenomena of small debris flows and small rock falls, which cannot be mapped individually but were included within areas with widespread landslides (**Figure 5D**, Section 4.4). Finally, sackungs are poorly represented in our study area.
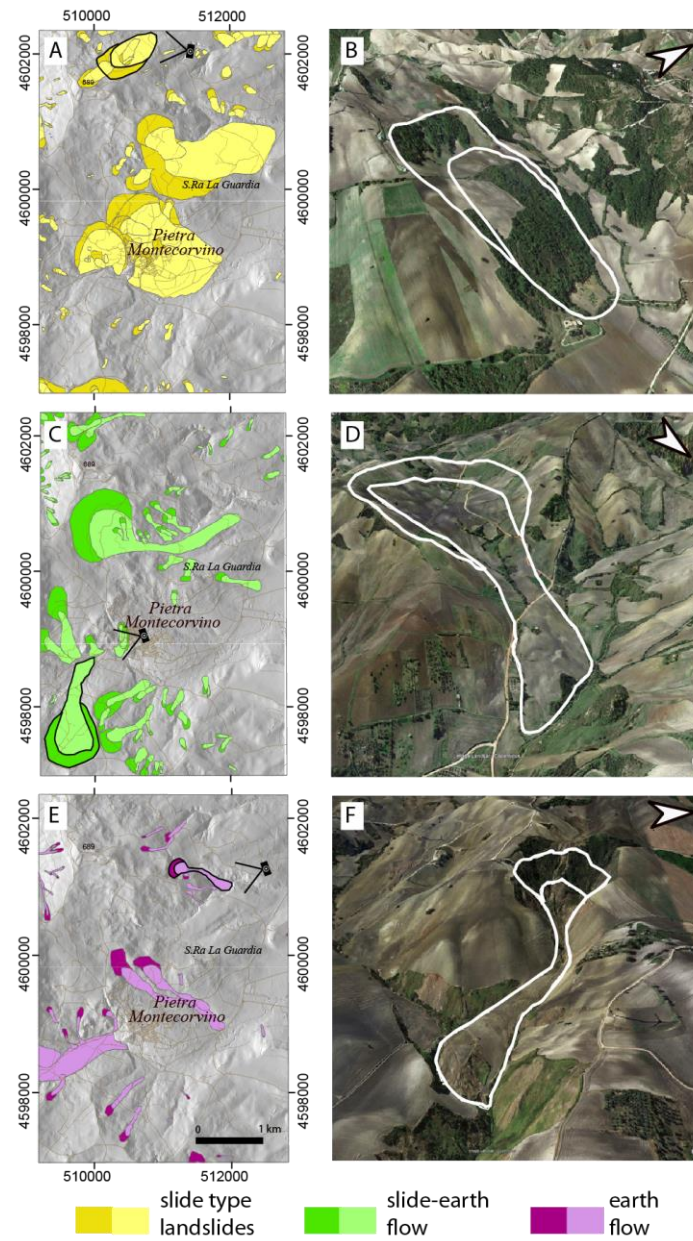
Figure 6. Examples in map (left column) and on © GoogleEarth™. images (right column) of slide type failures (A,B), slide-earthflow landslides (C,D), earthflows (E,F). For each row, black outlined polygons and camera symbols in the left image identify the landslide shown in the corresponding image on the right and the point of view, respectively.

4.3 Landslide estimated depth

The estimated depth of a landslide is assigned based on the main morphological characteristics of the landslide, such as: slope height, and extent of curvatures along the slope (convexity and concavity). Based on these morphological characteristics, landslides were classified as deep-seated or shallow.

Deep-seated landslides are predominantly represented by failures that cover considerable extents, even exceeding one square kilometre. Many of the deep-seated landslides can be classified as very old relict, very old and old. They often involve considerable volumes of material, and can alter the local morphology and geological structure. In the inventory map, deep-seated landslides are represented with two polygons, distinguishing the deposit area from the scarp area.

Shallow landslides are generally small (~10^4 m^2) and mainly represented by slide type and flow type landslides. They are generally characterised by a scarp not very pronounced, with an estimated height of less than 2 metres, and by a deposit without evident concavities and convexities on its surface. In the inventory, shallow landslides are mapped as single polygons including both the scarp and the deposit area.

4.4 Widespread landslides

The areas of widespread landslides (**Table 2**, **Figure 5D**) are represented by landslides which size is smaller than the smallest feature that can be represented at the publication scale of the final map. In the map we distinguished between: i) shallow earth/soil slides and earth flows, ii) debris flows, iii) rock falls. Their spatial distribution is mainly related to locally steep slopes, for instance in the vicinity of badlands, in the crown areas of pre-existing large landslides, or along the edges of ancient suspended fluvial terraces (**Figure 7**). Widespread shallow slides and flows typically involve weathered clayey soils, while widespread debris flows and rock falls are commonly fed by loose debris or poorly cemented conglomerates and breccias. Finally, it was not possible to assign a well-defined age to widespread landslides, although their morphological evidence suggests seasonal reactivations.

4.5 Descriptive statistics of the G-LIM

Descriptive statistics of landslide number and size are shown in **Figure 7**. Box plots in **Figure 7A, B** show the distribution of landslide areas for the landslide classified based on the expected relative age (**Figure 7A**) and the type of movement (**Figure 7B**).

Inspection of the plot in **Figure 7A** confirms that slides, slide-earth flows and flows are the most represented landslides of the inventory. Among these three classes, the slide type landslides are characterised by the largest size variability, while the slide earth flows are on average slightly larger than the others. In the plot of **Figure 7A**, landslides (on the left) are separated by areas of widespread landslides (on the right) because the latter are not related to a single feature and cannot be directly compared to single landslides. This is the reason why the areas of widespread landslides are on average larger than the single

319 landslides. In particular, the areas of widespread soil slides and earth flows are larger than the others because they typically

320 involve edges of fluvial terraces characterised by strong lateral continuity.

321 The plot in **Figure 7B** shows the size distribution of the four relative age classes of landslides. The clear separation of the age

322 classes according to their median values is a statistically robust indication of the reliability of this landslide classification

323 strategy, which is underused in the landslide-oriented international literature.

324 Comparing **Figure 7A** and **7B**, it is worth noting that the median area of all landslide types is around 10^5 m^2, which corresponds

325 to the median area of the old landslides group. This was expected since this is the most represented landslide age class within

326 the inventory.

327 **Figure 7C** shows landslides count (represented by a colour gradient and labels) and cumulated area (proportional to circle

328 sizes), grouped by relative age classes and landslide type. Visual inspection of the plot reveals that relict and very old landslides

329 are not represented by small landslides, and in particular by debris flows and rock falls, which tend to be small and easily

330 obliterated by erosion and subsequent failures. Further evidence is that a large portion of the total landslide area is occupied

331 by few relict and very old kilometre-scale slope failures, whereas a decreasing trend both in cumulated area and total number

332 of landslides is evident through time for all landslide types within the old landslides age class. Such evidence suggests a size

333 threshold effect of previous landslides on subsequent slope movements, probably controlled by slope-scale morphological and

334 hydrological perturbations induced by the occurrence of the first failure.
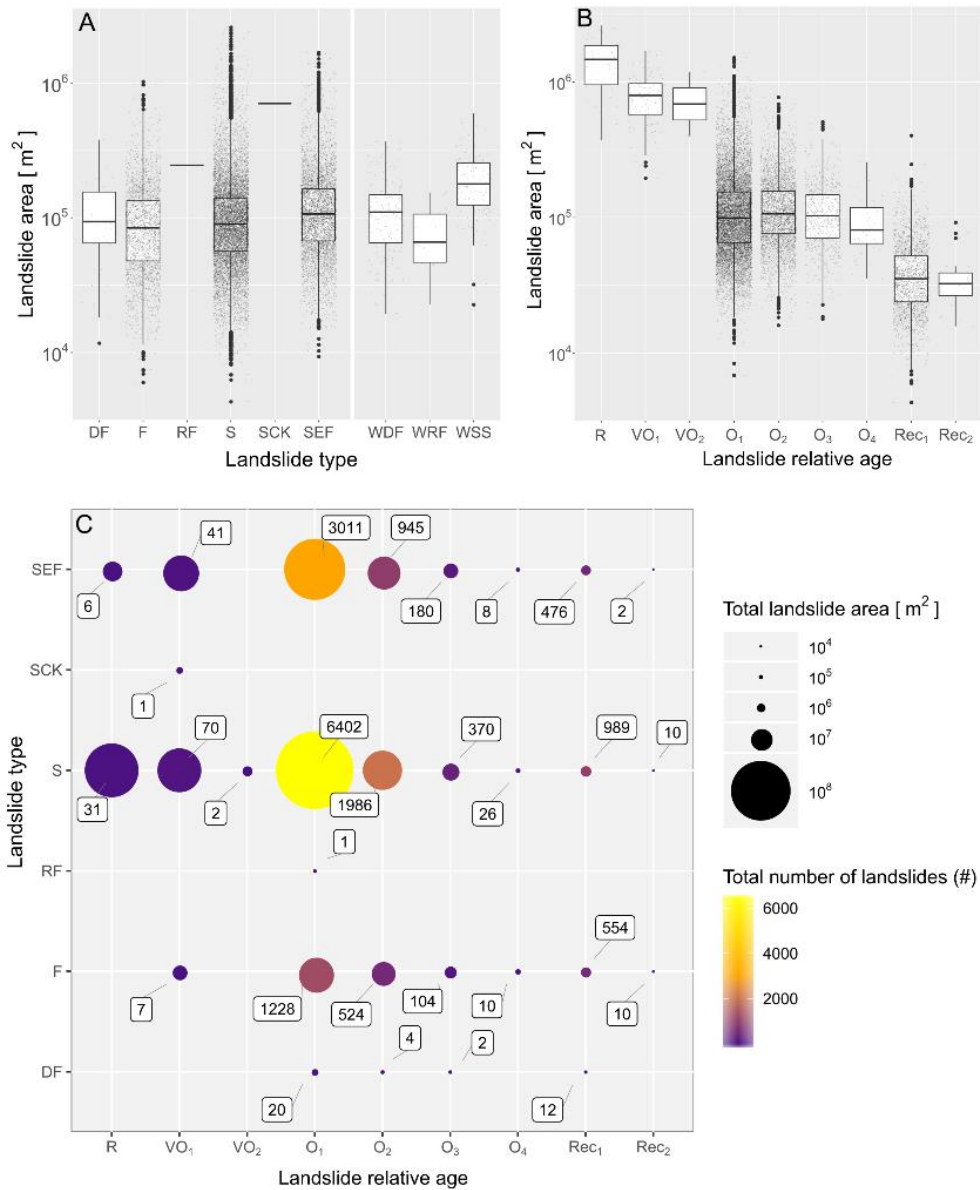
Figure 7. Plots summarising landslide statistics. (A) Landslides number (represented by a colour gradient and labels) and cumulated area (proportional to circle sizes), grouped by relative age classes and landslide type (SK, sackung; SEF, slide earth flow; S, slide; RF, rock fall; DF, debris flow; EF, earth flow). (B) Distribution of landslide areas within each relative age class. The relative age classes are indicated through a letter (R, relict; V, very old; and O, old), and a subscript number that indicates the generation within the age class (1–4). (C) Scatterplot showing cumulative size and count of landslides grouped by relative age in the abscissa and type in the ordinate. Landslide number is represented by a colour gradient and labels; total area is proportional to circle sizes.

335

4.6 Geomorphological elements

In the landslide inventory map, some geomorphological elements are also reported in addition to the mass movements (**Figure 8**). Such elements can be considered in relation with slope evolution and can provide useful information for landslide identification and mapping. In particular, our map includes alluvial deposits, fluvial terraces, and alluvial fans. Alluvial deposits are flat and always located in the lowest portions of the *Tavoliere delle Puglie* Plain and along the main water courses draining the hilly and mountain areas of the Daunia Apennine. Older alluvial/fluvial deposits are nowadays suspended over the present-day base level and are organised in fluvial terraces at different elevations, recording the ongoing deepening of the drainage network during the Quaternary. Alluvial fans were recognized and mapped in two relative age classes according to their appearance. They were classified as relict if dismantled and dissected due to the incision of the present-day river network. They were instead classified as recent if well preserved.
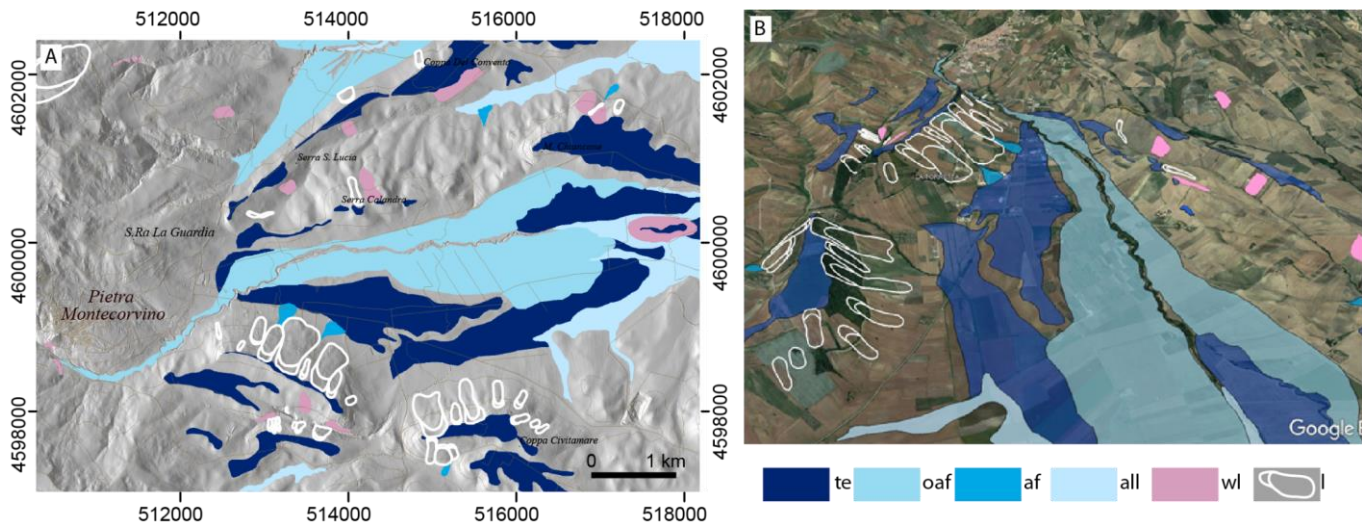
Figure 8 - (A) Excerpt of the landslide inventory map. Landslides were colored in white for enhancing the geomorphological elements. (B) Birds Eye view of the same area as (A) prepared using the ©GoogleEarth ™. In the legend: te, fluvial terrace; oaf, old alluvial fan; af, alluvial fan; all, alluvial deposits; wl, widespread landslides; l, landslide. ~~Figure 8 - (A) Excerpt of the landslide inventory map. Landslides were coloured in white for enhancing the geomorphological elements. (B) Birds Eye view of the same area as (A) prepared using © GoogleEarth™.~~

5 Conclusion

The landslide inventory map presented in this paper is a new catalogue of landslide phenomena in the Daunia Apennine. It provides new data uniformly distributed over the study area at an unprecedented cartographic detail.

The new landslide inventory map was produced upon request of the authorities of the Puglia Region, to solve the heterogeneity and limitations in the currently available landslide inventories (Pellicani et al., 2014b; Pellicani and Spilotro, 2015), mainly

353 due to: i) partial coverage of the territory, ii) heterogeneity in the degree of cartographic detail, iii) lack of metadata and other

354 methodological information, iv) geospatial inconsistencies where the different products overlap.

355 The new inventory represents a significant improvement upon earlier mapping because: (i) it presents a new homogeneous

356 landslide coverage for the Daunia Apennine, (ii) it is acquired with a uniform method and based on rigorous and reproducible

357 criteria, (iii) it keeps the same cartographic detail throughout the entire area, and (iv) it presents a systematic classification of

358 landslides by type, relative age, and depth, hence providing basic information at 1: 5000 scale for landslide characterization

359 and related land management activities. In addition, the spatially distributed information on landslide coverage portrayed in

360 the map, and the detailed scale of mapping, provide the fundamental information for landslide susceptibility and hazard

361 assessment (Guzzetti et al., 2005), and for supporting and integrating the study of seismic microzonation and the assessing of

362 seismic hazard both in urban and rural areas (Vignaroli et al., 2019). In addition to the technical and land management benefits,

363 our inventory provides new data to further investigation of the Quaternary evolution of the landscape of this part of the

364 Southern Apennines.

365 Analysis of the data revealed that the great majority of landslide volume was mobilised by relict and very old landslides,

366 whereas the landslide maximum size decreased over time and tended to cluster around pre-existing failures. The results have

367 relevance to determine the statistics of landslide size (Malamud et al., 2004), and to trigger detailed studies on the types,

368 patterns, and distribution of landslides in relation to geology (Bucci et al., 2016b) structure (Bucci et al., 2013), tectonic (Bucci

369 et al., 2014) and climatic forcing (Schiattarella et al., 2017). The presented dataset also documents the relationships between

370 landslides and other geomorphological elements, in particular with ancient and recent alluvial deposits and alluvial fans. These

371 fluvial related landforms can be used as input data to study quaternary depositional (Mirabella et al., 2018) and erosional events

372 (Mancini et al., 2020), and in combination with landslide information, to study the interplay of gravitational and fluvial

373 processes (Santangelo et al., 2013).

374 In the G-LIM presented, the vast majority of landslides are slow-moving, whereas rapid and fast landslides are rare (debris

375 flows and rock falls). Such evidence should be further confirmed by in-depth studies (e.g. multi-temporal inventories or

376 susceptibility models) as it may indicate a relatively low exposure of human life compared to other mountain areas of Southern

377 Apennines. On the other hand, it must be taken into account that the increasing frequency of extreme rainfall events may

378 trigger rapid and fast moving landslides also in this area, differently from what was observed in the past. This aspect further

379 shows that systematic landslide mapping to prepare new inventories and update the existing ones is crucial, particularly in the

380 ongoing climate change scenario (Donnini et al., under review).

381 We acknowledge that scarcity of data represents a limitation and a challenge for the landslide community. Most regional-scale

382 studies are less effective (or analysed) than expected due to the lack of easy sharing of landslide information in digital format.

Our work is also intended as a contribution to the broader geomorphological community, promoting the sharing of landslide dataset at regional scale from various environments.

Finally, it is worth reminding that a landslide map, even if accurate, does not answer all questions regarding hazards or risk at any scale. A Landslide map is informative about the area covered by landslides, but nothing can be said about the remaining territory. The map dataset should be used as an indication to optimise resources and to plan investigations aimed at determining landslide hazard and risk at a larger scale. In our case, the map dataset is published at 1: 5000 scale, and should be consulted at most at the same detail level.

6 Authors contributions

We declare that all authors' contributions in preparing both the dataset and the manuscript are equivalent to that of a first author. This is why all authors appear in alphabetical order.

7 Acknowledgments

This work was supported by the Civil Protection of the Puglia region, in the framework of the project "*Integrated assessment of geo-hydrological instability phenomena in the Apulia region, interpretative models and definition of rainfall thresholds for landslide triggering*" funded by the P.O.R. Puglia 2014-2020, Asse V - Azione 5.1. (Project identification number: B82F16003840006).

8 Data availability

Dataset is available at: https://doi.pangaea.de/10.1594/PANGAEA.942427 (Cardinali et al., 2022).

Competing interests

 The authors declare that they have no conflict of interest.

References

Antonini, G., Ardizzone, F., Cardinali, M., Galli, M., Guzzetti, F., and Reichenbach, P.: Surface deposits and landslide inventory map of the area affected by the 1997 Umbria-Marche earthquakes, Bollettino della Società Geologica Italiana, Volume spe, 843–853, 2002.

Ardizzone, F., Basile, G., Cardinali, M., Casagli, N., Del Conte, S., Del Ventisette, C., Fiorucci, F., Garfagnoli, F., Gigli, G.,

410   Guzzetti, F., Iovine, G., Mondini, A. C., Moretti, S., Panebianco, M., Raspini, F., Reichenbach, P., Rossi, M., Tanteri,
411   L., and Terranova, O.: Landslide inventory map for the Briga and the Giampilieri catchments, NE Sicily, Italy, Journal
412   of Maps, 8, 176–180, https://doi.org/10.1080/17445647.2012.694271, 2012.

413   Ardizzone, F., Fiorucci, F., Santangelo, M., Cardinali, M., Mondini, A. C. A. C., Rossi, M., Reichenbach, P., Guzzetti, F.,
414   and Ardizzone F.: Very-High Resolution Stereoscopic Satellite Images for Landslide Mapping, in: Landslide Inventory
415   and Susceptibility and Hazard Zoning, Berlin, Heidelberg, Citation Key: CNRPRODOTTI89033, 95–101, 2013.

416   Brozzetti, F., Boncio, P., Lavecchia, G., and Pace, B.: Present activity and seismogenic potential of a low-angle normal fault
417   system (Città di Castello, Italy): Constraints from surface geology, seismic reflection data and seismicity,
418   Tectonophysics, 463, 31–46, https://doi.org/10.1016/j.tecto.2008.09.023, 2009.

419   Bucci, F., Cardinali, M., and Guzzetti, F.: Structural geomorphology, active faulting and slope deformations in the epicentre
420   area of the MW 7.0, 1857, Southern Italy earthquake, Physics and Chemistry of the Earth, Parts A/B/C, 63, 12–24,
421   https://doi.org/10.1016/j.pce.2013.04.005, 2013.

422   Bucci, F., Novellino, R., Tavarnelli, E., Prosser, G., Guzzetti, F., Cardinali, M., Gueguen, E., Guglielmi, P., and Adurno, I.:
423   Frontal collapse during thrust propagation in mountain belts: a case study in the Lucania Apennines, Southern Italy,
424   Journal of the Geological Society, 171, 571–581, https://doi.org/10.1144/jgs2013-103, 2014.

425   Bucci, F., Santangelo, M., Cardinali, M., Fiorucci, F., and Guzzetti, F.: Landslide distribution and size in response to
426   Quaternary fault activity: The Peloritani Range, NE Sicily, Italy, Earth Surface Processes and Landforms, 41,
427   https://doi.org/10.1002/esp.3898, 2016a.

428   Bucci, F., Mirabella, F., Santangelo, M., Cardinali, M., and Guzzetti, F.: Photo-geology of the Montefalco Quaternary Basin,
429   Umbria, Central Italy, Journal of Maps, 12, https://doi.org/10.1080/17445647.2016.1210042, 2016b.

430   Bucci, F., Santangelo, M., Fiorucci, F., Ardizzone, F., Giordan, D., Cignetti, M., Notti, D., Allasia, P., Godone, D.,
431   Lagomarsino, D., Pozzoli, A., Norelli, E., and Cardinali, M.: Geomorphologic landslide inventory by air photo
432   interpretation of the High Agri Valley (Southern Italy), Journal of Maps, 17, 376–388,
433   https://doi.org/10.1080/17445647.2021.1943552, 2021.

434   Cardinali, M., Antonini, G., Reichenbach, P., and Guzzetti, F.: Photo geological and landslide inventory map for the Upper
435   Tiber River basin, 2001.

436   Cardinali, M., Ardizzone, F., Bucci, F., Fiorucci, F., Pisano, L., Santangelo, M., and Zumpano, V.: Geomorphological
437   landslide inventory map of the Daunia Mountains, Southern Italian Apennines, PANGAEA [data set],
438   https://doi.pangaea.de/10.1594/PANGAEA.942427, 2022.

439   Ciarcia, S., Di Nocera, S., Matano, F., and Torre, Ma. L.: Evoluzione tettono-sedimentaria e paleogeografica dei depocentri
440   «wedge-top» nell'ambito del «foreland basin system» pliocenico dell'Appennino meridionale (settore Irpino-Dauno),
441   Boll. Soc. Geol. It., 122, 117–137, 2003.

442   Cotecchia, F., Santaloia, F., and Tagarelli, V.: Towards A Geo-Hydro-Mechanical Characterization of Landslide Classes:
443   Preliminary Results, Applied Sciences, 10, 7960, https://doi.org/10.3390/app10227960, 2020.

444   Cruden, D. M. and Varnes, D. J.: Landslide Types and Processes, Special Report National Research Council Transportation
445   Research Board, 247, 36–75, 1996.

446   di Lernia, A., Cotecchia, F., Elia, G., Tagarelli, V., Santaloia, F., and Palladino, G.: Assessing the influence of the hydraulic
447   boundary conditions on clay slope stability: The Fontana Monte case study, Engineering Geology, 297, 106509,
448   https://doi.org/10.1016/j.enggeo.2021.106509, 2022.

449   Donnini, M., Napolitano, E., Salvati, P., Ardizzone, F., Bucci, F., Fiorucci, F., Santangelo, M., Cardinali, M., and Guzzetti,
450   F.: Impact of event landslides on road networks: a statistical analysis of two Italian case studies, Landslides, 14, 1521–
451   1535, https://doi.org/10.1007/s10346-017-0829-4, 2017.

452   Donnini, M., Santangelo, M., Gariano, S.L., Bucci, F., Peruccacci, S., Alvioli M., Althuwaynee, O., Ardizzone, F., Bianchi,
453   C., Bornaetxea, T., Brunetti, M.T., Cardinali, M., Esposito, G., Grita, S., Marchesini, I., Melillo, M., Salvasti, P.,
454   Yazdani, M., Fiorucci, F.: Landslides triggered by an extraordinary rainfall event in Central Italy on September 15,
455   2022, under review.

456   Filice, F. and Seeber, L.: The Culmination of an Oblique Time-Transgressive Arc Continent Collision: The Pollino Massif
457   Between Calabria and the Southern Apennines, Italy, Tectonics, 38, 3261–3280,
458   https://doi.org/10.1029/2017TC004932, 2019.

459   Fiorucci, F., Ardizzone, F., Rossi, M., and Torri, D.: The Use of Stereoscopic Satellite Images to Map Rills and Ephemeral

460   Gullies, Remote Sensing, 7, 14151–14178, https://doi.org/10.3390/rs71014151, 2015.

461   Fiorucci, F., Giordan, D., Santangelo, M., Dutto, F., Rossi, M., and Guzzetti, F.: Criteria for the optimal selection of remote
462   sensing images to map event landslides, Risk Assessment, Mitigation and Adaptation Strategies, Socioeconomic and
463   Management Aspects, https://doi.org/10.5194/nhess-2017-111, 2017.

464   Fiorucci, F., Giordan, D., Santangelo, M., Dutto, F., Rossi, M., and Guzzetti, F.: Criteria for the optimal selection of remote
465   sensing optical images to map event landslides, 405–417, https://doi.org/10.5194/nhess-18-405-2018, 2018.

466   Froude, M. J. and Petley, D. N.: Global fatal landslide occurrence from 2004 to 2016, Natural Hazards and Earth System
467   Sciences, 18, 2161–2181, https://doi.org/10.5194/nhess-18-2161-2018, 2018.

468   Galli, M., Ardizzone, F., Cardinali, M., Guzzetti, F., and Reichenbach, P.: Comparing landslide inventory maps,
469   Geomorphology, 94, 268–289, https://doi.org/10.1016/j.geomorph.2006.09.023, 2008.

470   Gioia, D., Di Leo, P., Giano, S. I., and Schiattarella, M.: Chronological constraints on a Holocene landslide in an
471   intermontane basin of the southern Apennines, Italy: Morphological evolution and palaeoclimate implications, The
472   Holocene, 21, 263–273, https://doi.org/10.1177/0959683610378879, 2011.

473   Guzzetti, F., Reichenbach, P., Cardinali, M., Galli, M., and Ardizzone, F.: Probabilistic landslide hazard assessment at the
474   basin scale, Geomorphology, 72, 272–299, https://doi.org/10.1016/j.geomorph.2005.06.002, 2005.

475   Guzzetti, F., Mondini, A. C., Cardinali, M., Fiorucci, F., Santangelo, M., and Chang, K.-T.: Landslide inventory maps: New
476   tools for an old problem, Earth-Science Reviews, 112, 42–66, https://doi.org/10.1016/j.earscirev.2012.02.001, 2012.

477   Harp, E. L. and Jibson, R. W.: Inventory of landslides triggered by the 1994 Northridge, California earthquake,
478   https://doi.org/10.5066/F7Z60MKF, 2017.

479   Hungr, O., Leroueil, S., and Picarelli, L.: The Varnes classification of landslide types, an update, Landslides, 11, 167–194,
480   https://doi.org/10.1007/s10346-013-0436-y, 2014.

481   Keaton, J. R. and DeGraff, J. V.: Surface observation and geologic mapping, in: Landslides: Investigation and mitigation.,
482   1996.

483   Losacco, N., Bottiglieri, O., Santaloia, F., Vitone, C., and Cotecchia, F.: The Geo-Hydro-Mechanical Properties of a
484   Turbiditic Formation as Internal Factors of Slope Failure Processes, Geosciences, 11, 429,
485   https://doi.org/10.3390/geosciences11100429, 2021.

486   Malamud, B. D., Turcotte, D. L., Guzzetti, F., and Reichenbach, P.: Landslide inventories and their statistical properties,
487   Earth Surf. Process. Landforms, 29, 687–711, https://doi.org/10.1002/esp.1064, 2004.

488   Mancini, M., Vignaroli, G., Bucci, F., Cardinali, M., Cavinato, G. P., Di salvo, C., Giallini, S., Moscatelli, M., Polpetta, F.,
489   Putignano, M. L., Santangelo, M., and Sirianni, P.: New stratigraphic constraints for the Quaternary source-to-sink
490   history of the Amatrice Basin (central Apennines, Italy), Geological Journal, 55, 4226–4251,
491   https://doi.org/10.1002/gj.3672, 2020.

492   Mirabella, F., Bucci, F., Santangelo, M., Cardinali, M., Caielli, G., De Franco, R., Guzzetti, F., and Barchi, M. R.: Alluvial
493   fan shifts and stream captures driven by extensional tectonics in central Italy, Journal of the Geological Society,
494   jgs2017-138, https://doi.org/10.1144/jgs2017-138, 2018.

495   Mondini, A. C., Chang, K., Rossi, M., Marchesini, I., and Guzzetti, F.: Semi-automatic recognition and mapping of event-
496   induced landslides by exploiting multispectral satellite images and DEM in a Bayesian framework, 852415,
497   https://doi.org/10.1117/12.977432, 2012.

498   Niculiţă, M., Mărgărint, M. C. M. C., and Santangelo, M.: Archaeological evidence for Holocene landslide activity in the
499   Eastern Carpathian lowland, Quaternary International, 415, http://dx.doi.org/10.1016/j.quaint.2015.12.048, 2016.

500   Pánek, T., Hartvich, F., Jankovská, V., Klimeš, J., Tábořík, P., Bubík, M., Smolková, V., and Hradecký, J.: Large Late
501   Pleistocene landslides from the marginal slope of the Flysch Carpathians, Landslides, 11, 981–992,
502   https://doi.org/10.1007/s10346-013-0463-8, 2014.

503   Pellicani, R. and Spilotro, G.: Evaluating the quality of landslide inventory maps: comparison between archive and surveyed
504   inventories for the Daunia region (Apulia, Southern Italy), Bull Eng Geol Environ, 74, 357–367,
505   https://doi.org/10.1007/s10064-014-0639-z, 2015.

506   Pellicani, R., Van Westen, C. J., and Spilotro, G.: Assessing landslide exposure in areas with limited landslide information,
507   Landslides, 11, 463–480, https://doi.org/10.1007/s10346-013-0386-4, 2014a.

508   Pellicani, R., Frattini, P., and Spilotro, G.: Landslide susceptibility assessment in Apulian Southern Apennine: heuristic vs.
509   statistical methods, Environ Earth Sci, 72, 1097–1108, https://doi.org/10.1007/s12665-013-3026-3, 2014b.

Petley, D.: Global patterns of loss of life from landslides, Geology, 40, 927–930, https://doi.org/10.1130/G33217.1, 2012.

Razak, K. A., Santangelo, M., Westen, C. J. V., Straatsma, M. W., and Jong, S. M. D.: Generating an optimal DTM from airborne laser scanning data for landslide mapping in a tropical forest environment, Geomorphology (Amst.), 190, 112–125, https://doi.org/10.1016/j.geomorph.2013.02.021, 2013.

Santangelo, M., Gioia, D., Cardinali, M., Guzzetti, F., and Schiattarella, M.: Interplay between mass movement and fluvial network organization: An example from southern Apennines, Italy, Geomorphology (Amst.), 188, 54–67, https://doi.org/10.1016/j.geomorph.2012.12.008, 2013.

Santangelo, M., Gioia, D., Cardinali, M., Guzzetti, F., and Schiattarella, M.: Landslide inventory map of the upper Sinni River valley, Southern Italy, Journal of Maps, 11, 444–453, https://doi.org/10.1080/17445647.2014.949313, 2015.

Santangelo, M., Cardinali, M., Bucci, F., Fiorucci, F., and Mondini, A. C.: Exploring event landslide mapping using Sentinel-1 SAR backscatter products, Geomorphology, 397, 108021, https://doi.org/10.1016/j.geomorph.2021.108021, 2022.

Schiattarella, M., Di Leo, P., Beneduce, P., and Ivo Giano, S.: Quaternary uplift vs tectonic loading: a case study from the Lucanian Apennine, southern Italy, Quaternary International, 101–102, 239–251, https://doi.org/10.1016/S1040-6182(02)00126-X, 2003.

Schiattarella, M., Giano, S. I., and Gioia, D.: Long-term geomorphological evolution of the axial zone of the Campania-Lucania Apennine, southern Italy: a review, Geologica Carpathica, 68, 57–67, https://doi.org/10.1515/geoca-2017-0005, 2017.

Schulz, W. H.: Landslides mapped using LIDAR imagery, Seattle, Washington, 2004.

Spalluto, L., Fiore, A., Miccoli, M. N., and Parise, M.: Activity maps of multi-source mudslides from the Daunia Apennines (Apulia, southern Italy), Nat Hazards, 106, 277–301, https://doi.org/10.1007/s11069-020-04461-3, 2021.

Thiery, Y., Terrier, M., Colas, B., Fressard, M., Maquaire, O., Grandjean, G., and Gourdier, S.: Improvement of landslide hazard assessments for regulatory zoning in France: STATE–OF–THE-ART perspectives and considerations, International Journal of Disaster Risk Reduction, 47, 101562, https://doi.org/10.1016/j.ijdrr.2020.101562, 2020.

Van Den Eeckhaut, M., Poesen, J., Verstraeten, G., Vanacker, V., Nyssen, J., Moeyersons, J., Beek, L. P. H. van, and Vandekerckhove, L.: Use of LIDAR-derived images for mapping old landslides under forest, Earth Surface Processes and Landforms, 32, 754–769, https://doi.org/10.1002/esp.1417, 2007.

Vignaroli, G., Mancini, M., Bucci, F., Cardinali, M., Cavinato, G. P., Moscatelli, M., Putignano, M. L., Sirianni, P., Santangelo, M., Ardizzone, F., Cosentino, G., Di Salvo, C., Fiorucci, F., Gaudiosi, I., Giallini, S., Messina, P., Peronace, E., Polpetta, F., Reichenbach, P., Scionti, V., Simionato, M., and Stigliano, F.: Geology of the central part of the Amatrice Basin (Central Apennines, Italy), Journal of Maps, 15, 193–202, https://doi.org/10.1080/17445647.2019.1570877, 2019.

Vitale, S. and Ciarcia, S.: Tectono-stratigraphic and kinematic evolution of the southern Apennines/Calabria–Peloritani Terrane system (Italy), Tectonophysics, 583, 164–182, https://doi.org/10.1016/j.tecto.2012.11.004, 2013.

Vitale, S., Ciarcia, S., Mazzoli, S., and Zaghloul, M. N.: Tectonic evolution of the 'Liguride' accretionary wedge in the Cilento area, southern Italy: A record of early Apennine geodynamics, Journal of Geodynamics, 51, 25–36, https://doi.org/10.1016/j.jog.2010.06.002, 2011.

Wasowski, J., Lamanna, C., and Casarano, D.: Influence of land-use change and precipitation patterns on landslide activity in the Daunia Apennines, Italy, Quarterly Journal of Engineering Geology and Hydrogeology, 43, 387–401, https://doi.org/10.1144/1470-9236/08-101, 2010.

Wasowski, J., Lamanna, C., Gigante, G., and Casarano, D.: High resolution satellite imagery analysis for inferring surface–subsurface water relationships in unstable slopes, Remote Sensing of Environment, 124, 135–148, https://doi.org/10.1016/j.rse.2012.05.007, 2012.

WP/WLI: International Geotechnical societies UNESCO Working Party on World Landslide Inventory. Multilingual landslide glossary, Richmond: BiTech Publishers Ltd, 1993.

Zumpano, V., Ardizzone, F., Bucci, F., Cardinali, M., Fiorucci, F., Parise, M., Pisano, L., Reichenbach, P., Santaloia, F., Santangelo, M., Wasowski, J., and Lollino, P.: The relation of spatio-temporal distribution of landslides to urban development (a case study from the Apulia region, Southern Italy), Journal of Maps, 0, 1–8, https://doi.org/10.1080/17445647.2020.1746417, 2020.

Appendix A

In the first phase of work, information and cartographic/thematic products were collected to support the preparation of the geomorphological landslide inventory map of the Daunia Apennines. Some of the listed products have been provided by the Regione Puglia, others can be consulted on the web, through Cartographic Portals or Web servers:

- Regional Technical Maps in digital format at a scale of 1:5,000, supplied by Regione Puglia (www.sit.puglia.it);

- Geological maps at scale 1:50.000 (CARG), available on the ISPRA cartographic portal;

- Geological maps at a scale of 1:100,000 (Geological Map of Italy), available on the ISPRA cartographic portal;

- Hydrogeomorphological map in scale 1:25.000 available on the SIT site of the Regione Puglia (http://webapps.sit.puglia.it/freewebapps/Idrogeomorfologia/index.html);

- Digital Elevation Model (DEM, cell 8×8m) provided by Regione Puglia (www.sit.puglia.it);

- Digital Elevation Model (DEM) made by LiDAR (1×1m cell), carried out within the framework of the Extraordinary Plan for Environmental Remote Sensing (PST-A) and provided by the Ministry of Ecological Transition (MiTE).

- Urbanised and land use maps, provided by the Regione Puglia (www.sit.puglia.it);

- Orthophoto maps provided by the Regione Puglia (www.sit.puglia.it);

- Landslide inventory maps of Apulia from:

  - *IFFI Inventory*: Inventory of Phenomena Franosi in Italy, compiled by ISPRA;

  - **Official Archives**: *Piano Stralcio per l'Assetto Idrogeologico* (PAI) of the Basin Authorities of Puglia, Basilicata, of the Rivers Trigno, Biferno and minor Saccione and Fortore, and of the Rivers Liri-Garigliano and Volturno; *Project Inventory of Phenomena Franosi in Italy (IFFI - update 2006)*, compiled by ISPRA; *Census Project of Italian Areas Historically Vulnerated by Geological and Hydraulic Disasters (AVI)*, drawn up by the National Group for Defence against geo-hydrological Disasters of the National Research Council (GNDCI-CNR);

  - **AdBP photo interpretation**: landslides from the photo interpretation study conducted by AdBP (Basin Authority of Puglia Region);

  - **Province of Foggia**: it deals with the landslides surveyed by the Province of Foggia within the framework of the agreements signed with the AdBP concerning the "Activity of collection and classification of data on landslide phenomena in the Province of Foggia" and "Conduct of studies for the deepening of the aspects related to the classified landslide phenomena".